Raman-induced phase conjugation spectroscopy

S. K. Saha and R. W. Hellwarth
Departments of Physics and Electrical Engineering, University of Southern California, Los Angeles, California 90089-0484
(Received 25 October 1982)

Complete Raman spectra of transparent media are obtained with a single 10-nsec, 10-mJ, laser pulse by a new spectroscopic technique which exploits resonant behavior of nondegenerate four-wave mixing in the phase-conjugate geometry.

To obtain optical Raman (Brillouin, etc.) spectra of transient media, hot media (above 10^{-3} K), or static media exhibiting strong fluorescence, or to obtain spectral resolution of greater than 1 cm^{-1}, one must generally employ some form of coherent Raman spectroscopy (CRS). The most widely used CRS techniques employ two coherent sources whose frequencies are separated by nearly the Raman excitation frequency. These techniques include (1) stimulated Raman gain (loss) spectroscopy (SRS),[1-5] (2) coherent anti-Stokes Raman scattering (CARS),[4-8] (3) Raman-induced Kerr effect (RIKE),[4,5,7,9] and two-beam interferometry.[4,7,10]

Here we propose and demonstrate a new CRS technique that also employs coherent sources at only two frequencies. This is a form of four-wave mixing in which two beams at ω and at $\omega-w$ (or at $\omega+w$) mix with a third beam at ω to generate a fourth beam at $\omega-w$ (or at $\omega+w$). The generated beam is nearly phase conjugate to one of the beams at ω. This effect, which we call "Raman-induced phase conjugation" or RIPC has the following characteristics. (1) The Raman signal is generated as a coherent beam which is nearly phase conjugate to one of the incident beams. (2) Up to 16 independent combinations of beam polarizations are possible. (3) The Raman signal beam is not coincident with any input beam. (4) Phase matching among the four beams can be achieved for excitation frequencies in a wide range (many hundreds of cm^{-1}) for a given beam geometry. (5) Phase matching among the four beams can also be achieved, for given beam frequencies, for a wide range of input, or "image," beam angles, thus allowing an enhanced (or altered) phase-conjugate image at Raman resonance. This spatial resolution can be used to enhance spectral resolution or to focus on a particular region of the sample. (6) The wave vectors of excitations observed in RIPC are nearly $(2\omega \pm w)n/c$ where n is the refractive index. (7) If the input beam containing $\omega \pm w$ is broadband, and beam polarizations are properly adjusted, only Raman-shifted frequencies will be conjugated, and the usual nonresonant component will be absent. These properties allow Raman spectra to be recorded with single ($\sim$ nsec) pulses. After describing our initial results and theory, we note how RIPC may be superior to all other CRS techniques in special situations, such as for hot, birefringent, and slightly tremulous media.

A typical experimental arrangement for recording (a large range of) the Raman spectrum with a single 10-nsec pulse by RIPC is shown in Fig. 1. Here a Raman vibration(s) of frequency w in the medium S is excited by the simultaneous presence of the monochromatic beam 2 at ω and the spectral component of the broadband beam 3 that is within a Raman linewidth of $\omega-w$ (or of $\omega+w$ if the broadband source is at higher frequency than beam 1). This excitation varies the optical polarizability seen by monochromatic beam 1 (at ω), scattering a portion of it into beam 4, which becomes the signal at fre-

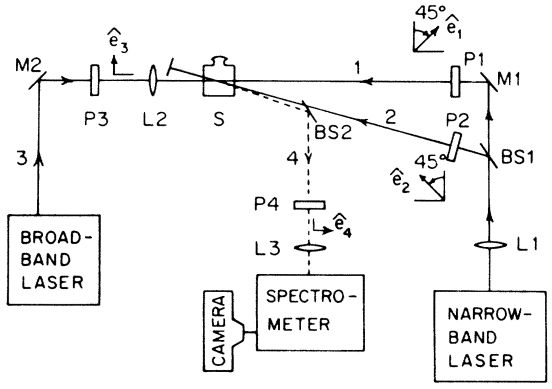

FIG. 1. Schematic of apparatus used to observe RIPC. Incident beams 1, 2, and 3 are polarized by polarizers $P1$, $P2$, and $P3$. Output signal beam 4 is analyzed by polarizer $P4$. Polarizations are either as shown (relative to the same plane in S) or modified as described in text. Incident beams were focused by lenses $L1$ (1-m focal length) and $L2$ (30-cm focal length) into the 1-cm long sample cell S.

quency $\omega - w$ whose phase front is nearly conjugate to that of beam 2 at the cell entrance plane. Some typical spectrometer traces of beam 4 are shown in Fig. 2. For these spectra the beams 1 and 2 were each 10-mJ, 10-nsec pulses from a frequency-doubled Nd:YAG laser, half of whose output was used to pump the Rhodamine 6G dye laser which supplied beam 3 with $\sim$0.1-mJ, 8-nsec pulses of broadband radiation spanning about 500 cm^{-1}. The angle θ_{12} between beams 1 and 2 was $\sim$40 mrad. Phase matching optimized the signal when beam 3 was at an angle of 1 to 3 mrad from the direction counter to beam 1 (depending on w in the range 1000–3000 cm^{-1}). The observed signal spanning 300 cm^{-1} in Fig. 2(e) is well within the limit of 500 cm^{-1} set by phase matching. Also within limits is the image signal of Fig. 3 spanning $\sim$30 mrad. The limits set by phase matching can be estimated as follows.

Signals fall to half maximum whenever the magnitude Δk of the beam wave-vector mismatch $\Delta\vec{k} \equiv \vec{k}_1 - \vec{k}_2 + \vec{k}_3 - \vec{k}_4$ exceeds either $2.8/L$ (when the absorption coefficient α times the interaction length L is less than 1) or α (when $\alpha L > 1$). Consider nearly collinear and counterpropagating monochromatic beams at ω and ν ($\sim\omega - w$) aligned for perfect phase match ($\Delta k = 0$) as in Fig. 1. Then, if only the angle of the input (image) beam 2 is varied by $\Delta\theta$ from the angle θ_{12} made with beam 1, the resulting Δk is ($k_2 \equiv \omega n_2/c$, etc.)

$$\Delta k \sim |\tfrac{1}{2}k_2(k_2/k_4 - 1)\theta_{12}\Delta\theta| \ . \tag{1}$$

For the case of Fig. 3, we expect from (1) that $\Delta\theta$ within $\pm$20 mrad will preserve phase matching. If, on the other hand, only the frequency ν of the pump beam 3 is varied by $\Delta\nu$ around perfect phase matching, one obtains

$$\Delta k \sim |(\theta_{34}^2 - 1 + k_4/k_3)n_3\Delta\nu/c| \ , \tag{2}$$

where θ_{34} is the angle between beams 3 and 4. From this, we expect in the situation of Fig. 2(e) that phase matching is achieved for $\Delta\nu/2\pi c$ within the range $\pm$200 cm^{-1}. These ranges are one to two orders of magnitude larger than are available in CARS spectroscopy.

The strength of the observed lines in Fig. 1 and the absence of background wave mixing off resonance in Figs. 1(a)–1(d) can be predicted from the dependence on the optical electric field $\vec{\mathscr{E}}(\vec{x},t)$ of that part $\vec{\mathscr{P}}^{(3)}(\vec{x},t)$ of the nonlinear optical polarization density that is third order in $\vec{\mathscr{E}}$. In liquids, gases, and glasses when the Born-Oppenheimer approximation is valid, i.e., when all optical frequencies are well below the electronic band edge, $\vec{\mathscr{P}}^{(3)}$ is of the form (with space argument $\vec{x}$ suppressed)[11,12]

$$\vec{\mathscr{P}}^{(3)}(t) = \tfrac{1}{2}\sigma\vec{\mathscr{E}}(t)\mathscr{E}^2(t) + \vec{\mathscr{E}}(t)\int_{-\infty}^{t} ds\, a(t-s)\mathscr{E}^2(s) + \int_{-\infty}^{t} ds\, b(t-s)\vec{\mathscr{E}}(t)\cdot\vec{\mathscr{E}}(s)\vec{\mathscr{E}}(s) \ . \tag{3}$$

Here σ is a real number measuring the instantaneous nonlinear electronic response or "hyperpolarizability" (that would be present if the nuclei were fixed), and $a(\tau)$ and $b(\tau)$ are nuclear response functions describing Raman-active excitations which alter the optical susceptibility. These "nuclear" terms may be thought of as of the linear form $\chi(t)\mathscr{E}(t)$ but with $\chi(t)$ modulated by nuclear motions (vibration, rotation, etc.) driven by the interaction potential $-\frac{1}{2}\chi\mathscr{E}^2(s)$ at past times.[11,12] In thermal media, the

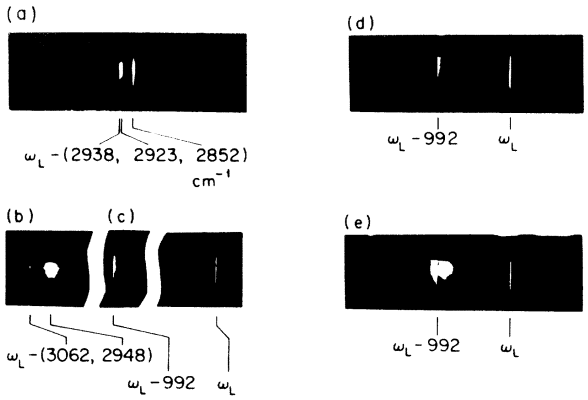

FIG. 2. Spectra taken with apparatus of Fig. 1. Samples S were (a) cyclohexane and (b)–(e) benzene. In (a)–(d) linear polarizers were fixed as shown in Fig. 1, but in (e) polarizer P_4 was rotated clockwise by $\theta \sim 10°$ from direction shown. Spectra (d) and (e) were taken with lower grating order. The cross sections of the three Raman lines in (a) are comparable. The cross sections of the Raman lines in (b) and (c) are in the ratio 0.01:0.1:1, respectively. Spectra were recorded on Polaroid 410 film. From one to ten pulses were used for exposure depending on line strength.

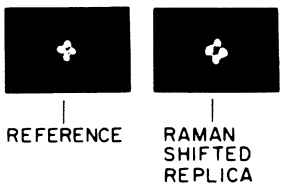

FIG. 3. Image replication. Images recorded on Polaroid 410 film at open exit slits of spectrometer when four-hole image plate was inserted adjacent to $P2$ in Fig. 1. Reference image obtained with plane mirror in place of cell S. This frequency-shifted replica was obtained with benzene in cell S and all beams as in Fig. 1. Image subtended 30 mrad at sample.

response functions $a(\tau)$ and $b(\tau)$ are related to the differential Raman scattering cross sections

$$d^2\sigma_i(\Delta)/d\Omega\, d\Delta$$

[$\mathrm{cm}^{-1}\,\mathrm{sr}^{-1}\,(\mathrm{rad/s})^{-1}$] which give the probability per unit length for a photon to scatter from frequency ω to frequency $\nu=\omega-\Delta$ per unit (angular) frequency range per unit solid angle for scattered polarization either parallel ($i=||$) or perpendicular ($i=\perp$) to the incident beam polarization. Defining the Fourier transforms

$$A_\Delta \equiv \int_0^\infty dt\, a(t)e^{i\Delta t}$$

and similarly for B_Δ, we have[11,12]

$$\mathrm{Im}B_\Delta = \frac{\pi c^4}{\hbar\omega\nu^3}\frac{d^2\sigma_\perp}{d\Omega\, d\Delta}(1-e^{-\hbar\Delta/kT}) \tag{4}$$

and a similar relation with A_Δ and $\frac{1}{2}\sigma_{||}-\sigma_\perp$ substituted for B_Δ and $\sigma_\perp$, respectively. Here kT is Boltzmann's constant times temperature. Because of the causal nature of $a(t)$ and $b(t)$ the real parts of A_Δ and B_Δ can be calculated from the imaginary parts (4) by the usual Kramers-Kronig integrals.[11] Given the Raman spectrum of a medium and the electronic hyperpolarizability σ, the nonlinear polarization density (3) is completely determined.

In our experiments $\vec{\mathscr{E}}$ in (3) is essentially the sum of three incident beams $\vec{\mathscr{E}}_1+\vec{\mathscr{E}}_2+\vec{\mathscr{E}}_3$ which give rise to a term in the polarization density $\vec{\mathscr{P}}^{(3)}$ which generates a fourth phase-conjugate beam $\vec{\mathscr{E}}_4$. Our results can be understood by assuming each beam is a plane wave:

$$\vec{\mathscr{E}}_1 = \mathrm{Re}\vec{\mathrm{E}}_1 e^{i\vec{k}_1\cdot\vec{x}-i\omega t},$$

etc. If one takes from (3) the part $(\mathrm{Re}\vec{\mathrm{P}}_4 e^{i\vec{k}_4\cdot\vec{x}-i\nu t})$ of $\vec{\mathscr{P}}^{(3)}$ which generates the signal (phase-conjugate) beam one finds that[12] ($\mu\equiv\nu-\omega=-\Delta$, $A_\mu=A_{-\Delta}=A_\Delta^*$, $A_0\equiv A_{\Delta=0}$, etc.)

$$\vec{\mathrm{P}}_4=\tfrac{1}{4}[\vec{\mathrm{E}}_1\vec{\mathrm{E}}_2^*\cdot\vec{\mathrm{E}}_3(\sigma+B_0+2A_\mu)+\vec{\mathrm{E}}_2^*\vec{\mathrm{E}}_1\cdot\vec{\mathrm{E}}_3(\sigma+B_0+B_\mu)+\vec{\mathrm{E}}_3\vec{\mathrm{E}}_2^*\cdot\vec{\mathrm{E}}_1(\sigma+2A_0+B_\mu)]e^{i\Delta\vec{k}\cdot\vec{x}}\,. \tag{5}$$

With the polarizers arranged as in Fig. 1, the effective polarization component is

$$P_{4h}\equiv\hat{h}\cdot\vec{\mathrm{P}}_4=(B_\mu-2A_\mu)E_1E_2^*E_3/8\,,$$

where $\hat{h}$ is a horizontal unit vector. Since B_μ and A_μ are only large near Raman resonances, we observe in Figs. 2(a)–2(d) narrow lines when $\Delta\sim w$ and negligible signal far from resonance. If the linear polarizer $\hat{e}_4$ is oriented at $\pi/4+\theta$ from $\hat{e}_1$, then one finds from (5) that the effective component of $\vec{\mathrm{P}}_4$ is $P_{4\theta}=P_{4h}\cos\theta+P_{4v}\sin\theta$, where

$$P_{4v}\equiv\hat{v}\cdot\vec{\mathrm{P}}_4 = (\sigma+B_0+\tfrac{1}{2}B_\mu+A_\mu)E_1E_2^*E_3/4\,,$$

and $\hat{v}$ is a unit vertical vector (parallel to $\hat{e}_3$). Evident in P_{4v} is the nonresonant (constant) background term which is observed in Fig. 2(e) to interfere with the resonant B_μ and A_μ terms when $\Delta\sim w$. Since the output signal intensity is proportional to $|\hat{e}_4^*\cdot\vec{\mathrm{P}}_4|^2$ in general, the details of this interference can be used to measure the parameters appearing in (5).[13]

If the incident beams are negligibly disturbed by the mixing process, the intensity I_4 of the phase-conjugate signal can be easily calculated from (5) in terms of the incident intensities I_1, I_2, and I_3. The result is often written in the form

$$I_4=\beta^2L^2I_1I_2I_3\,, \tag{6}$$

where L is an effective interaction length (equal to the cell length in our case) and β is a nonlinear coefficient which depends on all beam polarizations and the parameters in (5). For example, the magnitudes of the signals seen in Figs. 2(c) and 2(d) may be estimated using the foregoing relations and the measured values for the 992-cm^{-1} line of benzene: 1.6×10^{-8} for $d\sigma_{||}/d\Omega$, 1.2 cm^{-1} for the linewidth, and 0.02 for $\sigma_\perp/\sigma_{||}$.[14,15] These give $\beta\sim1$ cm/GW at line center. For our beam intensities, this predicts $I_4/I_2\sim10^{-5}$, which is consistent with our observations.

We summarize the properties of RIPC as a Raman spectroscopic tool by considering the following task, for which RIPC appears to be better suited than any other technique. Suppose one wished to obtain the Raman spectrum of a crystal in a phase that only exists at temperatures ($\gtrsim10^3$ K) that are too high for spontaneous Raman spectra to be visible in the thermal background.[16,17] Suppose further that the dispersion of the refractive index is unknown so that the CARS signal could not be obtained without a very tedious search for the phase-matching angle. Suppose also that the crystal is birefringent. Then a probe beam having comparable ordinary and extraordinary components (necessary for RIKE) cannot be nulled by any practical polarizer to better than $\sim1\%$. This would make RIKE insensitive to any but the strongest Raman lines. Suppose further that the hot crystal is undergoing temperature fluctuations. Raman gain spectroscopy and two-beam interferometry, which rely on many seconds of processing of very stable beams, become

inapplicable. Noise-initiated single-pass stimulated Raman scattering (ordinary SRS) might produce a signal, but only at the strongest Raman line, and provided that the crystal is not damaged by self-focusing before threshold is reached. However, none of these impediments would prevent RIPC spectra, such as those in Fig. 2, from being obtained.

The authors would like to acknowledge the support of the Air Force Office of Scientific Research under Grant No. 78-3478 and of the National Science Foundation under Grant No. ECS-8114828.

[1]W. J. Jones and B. P. Stoicheff, Phys. Rev. Lett. 13, 657 (1964).

[2]R. W. Hellwarth, Phys. Rev. 130, 1850 (1963).

[3]A. Owyoung, in *Advances in Infrared and Raman Spectroscopy,* edited by R. Clark and R. Hestor (Heyden, London, 1979), Vol. 9.

[4]A. Owyoung, in *Chemical Applications of Nonlinear Spectroscopy,* edited by A. Harvey (Academic, New York, 1979).

[5]S. A. Akhmanov, in *Nonlinear Spectroscopy, Proceedings of the International School of Physics, "Enrico Fermi,"* edited by N. Bloembergen (North-Holland, Amsterdam, 1977).

[6]P. D. Maker and R. W. Terhune, Phys. Rev. A 137, 801 (1965).

[7]G. L. Eesley, J. Quant. Spectrosc. Radiat. Transfer 22, 507 (1979).

[8]J. L. Oudar, R. W. Smith, and Y. R. Shen, Appl. Phys. Lett. 34, 758 (1979).

[9]D. Heiman, R. W. Hellwarth, M. D. Levenson, and G. Martin, Phys. Rev. Lett. 36, 189 (1976).

[10]A. Owyoung and P. S. Percy, J. Appl. Phys. 48, 674 (1977).

[11]R. W. Hellwarth, J. Cherlow, T. T. Yang, Phys. Rev. B 11, 964 (1975).

[12]R. W. Hellwarth, in *Progress in Quantum Electronics,* edited by J. H. Sanders and S. Stenholm (Pergamon, New York, 1977), Vol. 5, Part 1.

[13]S. K. Saha and R. W. Hellwarth (unpublished).

[14]J. G. Skinner and W. G. Nilsen, J. Opt. Soc. Am. 58, 113 (1968).

[15]Y. Kato and H. Takuma, J. Chem. Phys. 54, 5398 (1971).

[16]P. Alain, J. P. Coutures, and B. Piriou, J. Raman Spectrosc. 8, 88 (1979).

[17]A. Owyoung, IEEE J. Quantum Electron. QE-14, 192 (1978).

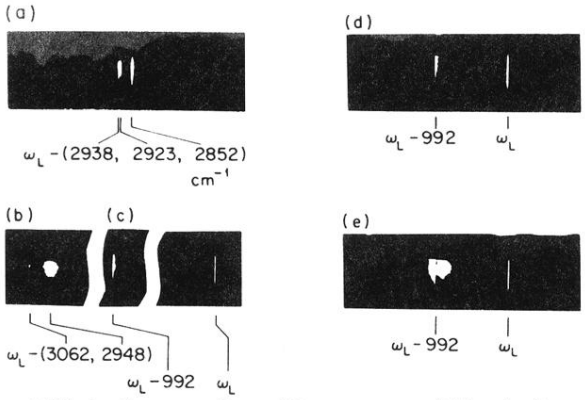

FIG. 2. Spectra taken with apparatus of Fig. 1. Samples S were (a) cyclohexane and (b)—(e) benzene. In (a)—(d) linear polarizers were fixed as shown in Fig. 1, but in (e) polarizer P_4 was rotated clockwise by $\theta \sim 10°$ from direction shown. Spectra (d) and (e) were taken with lower grating order. The cross sections of the three Raman lines in (a) are comparable. The cross sections of the Raman lines in (b) and (c) are in the ratio 0.01:0.1:1, respectively. Spectra were recorded on Polaroid 410 film. From one to ten pulses were used for exposure depending on line strength.

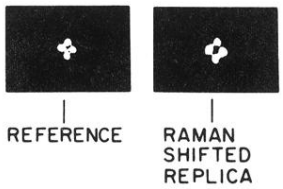

FIG. 3. Image replication. Images recorded on Polaroid 410 film at open exit slits of spectrometer when four-hole image plate was inserted adjacent to $P2$ in Fig. 1. Reference image obtained with plane mirror in place of cell S. This frequency-shifted replica was obtained with benzene in cell S and all beams as in Fig. 1. Image subtended 30 mrad at sample.